Numer. Math. Theor. Meth. Appl.
doi: 10.4208/nmtma.OA-2020-0155

Vol. **14**, No. 3, pp. 797-810
August 2021

Explicit Hybrid Numerical Method for the Allen-Cahn Type Equations on Curved Surfaces

Yongho Choi[1], Yibao Li[2], Chaeyoung Lee[3], Hyundong Kim[3] and Junseok Kim[3,*]

[1] *Department of Mathematics and Big Data, Daegu University, Gyeongsan-si, Gyeongsangbuk-do 38453, Republic of Korea*
[2] *School of Mathematics and Statistics, Xi'an Jiaotong University, Xi'an 710049, China*
[3] *Department of Mathematics, Korea University, Seoul 02841, Republic of Korea*

Received 4 October 2020; Accepted (in revised version) 24 January 2021

Abstract. We present a simple and fast explicit hybrid numerical scheme for the motion by mean curvature on curved surfaces in three-dimensional (3D) space. We numerically solve the Allen-Cahn (AC) and conservative Allen-Cahn (CAC) equations on a triangular surface mesh. We use the operator splitting method and an explicit hybrid numerical method. For the AC equation, we solve the diffusion term using a discrete Laplace-Beltrami operator on the triangular surface mesh and solve the reaction term using the closed-form solution, which is obtained using the separation of variables. Next, for the CAC equation, we additionally solve the time-space dependent Lagrange multiplier using an explicit scheme. Our numerical scheme is computationally fast and efficient because we use an explicit hybrid numerical scheme. We perform various numerical experiments to demonstrate the robustness and efficiency of the proposed scheme.

AMS subject classifications: 65M06, 65Z05, 68U20

Key words: Allen-Cahn equation, conservative Allen-Cahn equation, Laplace-Beltrami operator, triangular surface mesh, hybrid numerical method, PDE on surface.

1. Introduction

The Allen-Cahn (AC) equation was first proposed by Allen and Cahn in 1979 [1] as a mathematical model for antiphase domain coarsening in Fe-Al alloys

*Corresponding author.
Email addresses: yongho_choi@daegu.ac.kr (Y. Choi), cfdkim@korea.ac.kr (J.S. Kim)

$$\frac{\partial \phi(\mathbf{x},t)}{\partial t} = -\frac{F'(\phi(\mathbf{x},t))}{\epsilon^2} + \Delta\phi(\mathbf{x},t), \quad \mathbf{x} \in \Omega, \quad t > 0, \tag{1.1}$$

where $F(\phi) = 0.25(\phi^2 - 1)^2$ and ϵ is the gradient energy coefficient. Here, ϕ is the difference between the concentrations, i.e., $\phi = c_A - c_B$, where c_A and c_B are the mass fractions of components A and B in binary alloys. Therefore, the range of ϕ is $-1 \le \phi \le 1$. It is well known that the AC equation has a property that does not conserve the total mass. The $F(\phi)$ is Ginzburg-Landau double-well potential energy function with minimum values at -1 and 1 [12].

For the motion by mean curvature with conservation of area, the conservative AC (CAC) equation [4, 16] was proposed using the Lagrange multiplier, which depends on not only time but also space, and is given by

$$\frac{\partial \phi(\mathbf{x},t)}{\partial t} = -\frac{F'(\phi(\mathbf{x},t))}{\epsilon^2} + \Delta\phi(\mathbf{x},t) + \beta(t)\sqrt{F(\phi(\mathbf{x},t))}, \quad \mathbf{x} \in \Omega, \quad t > 0, \tag{1.2}$$

where $\Omega \subset \mathbb{R}^d$ is a domain, ϕ is the order parameter, $\sqrt{F(\phi)} = 0.5|\phi^2 - 1|$, ϵ is a constant related to the interfacial thickness, and $\beta(t)$ is given by

$$\beta(t) = \frac{\displaystyle\int_\Omega F'(\phi(\mathbf{x},t))d\mathbf{x}}{\epsilon^2\sqrt{\displaystyle\int_\Omega F(\phi(\mathbf{x},t))d\mathbf{x}}}. \tag{1.3}$$

It is well known that the non-standard time-space dependent Lagrange multiplier $\beta(t)\sqrt{F(\phi(\mathbf{x},t))}$ has a better area-preserving property than the standard time-only dependent Lagrange multiplier. Further explanation of its derivation can be found in [4].

In this study, we present a simple explicit hybrid numerical scheme for the AC type equations on curved surfaces in 3D space. First, let us consider the surface AC equation [31]

$$\frac{\partial \phi(\mathbf{x},t)}{\partial t} = -\frac{F'(\phi(\mathbf{x},t))}{\epsilon^2} + \Delta_{\mathcal{S}}\phi(\mathbf{x},t), \quad \mathbf{x} \in \mathcal{S}, \quad t > 0, \tag{1.4}$$

where $\mathcal{S}$ is a surface in $\mathbb{R}^3$. Here, $\Delta_{\mathcal{S}} = \nabla_{\mathcal{S}} \cdot \nabla_{\mathcal{S}}$ is the Laplace-Beltrami operator on $\mathcal{S}$ and $\nabla_{\mathcal{S}}$ is the surface gradient. One of the definitions of surface gradient uses a smooth extension [21]. Let $\mathcal{N}$ be a narrow embedding band around $\mathcal{S}$, i.e., $\mathcal{S} \subset \mathcal{N}$. Let $\phi_E : \mathcal{N} \to \mathbb{R}$ be a smooth extension of $\phi : \mathcal{S} \to \mathbb{R}$. Then, the surface gradient is defined as

$$\nabla_{\mathcal{S}}\phi := \nabla\phi_E - \frac{\nabla\psi}{|\nabla\psi|}\left(\frac{\nabla\psi}{|\nabla\psi|}\right)^T \nabla\phi_E, \tag{1.5}$$

where ψ is a function on $\mathcal{N}$ such that $\mathcal{S} = \{\mathbf{x} \in \mathcal{N} \,|\, \psi(\mathbf{x}) = 0\}$. Here, the gradient is a column vector. More details about the Laplace-Beltrami operator can be found in [21, 31]. The surface AC equation is a gradient flow in $L^2(\mathcal{S})$ for the total energy functional

$$\mathcal{E}(\phi) = \int_{\mathcal{S}} \left(\frac{F(\phi)}{\epsilon^2} + \frac{|\nabla_{\mathcal{S}}\phi|^2}{2}\right) dA. \tag{1.6}$$

It can be shown that $\mathcal{E}$ decreases over time, i.e.,

$$\frac{d\mathcal{E}(\phi)}{dt} = -\int_{\mathcal{S}} \phi_t^2 dA \leq 0. \tag{1.7}$$

The proofs of strong and global well-posedness related to the surface AC equation are presented in [7] and [17], respectively. The surface AC equation physically models the phase separation on surfaces [20]. In [31], the authors present the stabilized semi-implicit finite element method for the surface AC equation. Similarly, the surface CAC equation is defined as

$$\frac{\partial \phi(\mathbf{x},t)}{\partial t} = -\frac{F'(\phi(\mathbf{x},t))}{\epsilon^2} + \Delta_{\mathcal{S}}\phi(\mathbf{x},t) + \beta(t)\sqrt{F(\phi(\mathbf{x},t))}, \quad \mathbf{x} \in \mathcal{S}, \quad t > 0, \tag{1.8}$$

where $\beta(t)$ is given by

$$\beta(t) = \frac{\displaystyle\int_{\mathcal{S}} F'(\phi(\mathbf{x},t))dA}{\epsilon^2\sqrt{\displaystyle\int_{\mathcal{S}} F(\phi(\mathbf{x},t))dA}}. \tag{1.9}$$

There are many applications for solving partial differential equations on surfaces such as texture synthesis on arbitrary surfaces [29], phase separation patterns for di-block copolymers on spherical surfaces [28], denoising on the curved surfaces [2], cardiac electrophysiology in medicine [25], cell division [9], and pattern formation on animal skin [14]. Because it is not always possible to use analytic solutions on the surfaces, numerical analysis is required.

Various numerical methods have been introduced to approximate solutions of partial differential equations on surfaces. Macdonald and Ruuth presented the implicit closest point method to solve partial differential equations on surfaces [19]. Merriman and Ruuth [22] introduced a computational technique for the curvature-driven motion of a curve constrained to move on a given surface. Mohammadi *et al.* [23] used the radial basis function method to numerically solve the AC equation on surfaces. Furthermore, there exist many studies by using spectral element method [27], finite element method [5,8,11,31,32], finite difference method [13,18], finite volume method [28], closest point method [6,15,19], radial basis function [23], and linearly stabilized splitting scheme [30]. In [34], the authors present a new modeling of phase fields on deforming shell surfaces. The phase changes are modeled by the Cahn-Hilliard equation, coupled with nonlinear thin shell theory. Isogeometric finite elements were used, and a monolithic and fully implicit time-stepping method was used to solve the coupled system simultaneously.

We solve the AC and CAC equations on the triangular surfaces mesh using the explicit hybrid numerical method that was developed by Jeong and Kim [13] on the full computational domain (general Cartesian plane) and Choi *et al.* [6] on the narrow band domain. The contents of the paper are organized as follows. In Section 2, we present the numerical solution. In Section 3, we present numerical experiments. Finally, the conclusions are presented in Section 4.

2. Numerical solution

We use Xu's discretization of the Laplace-Beltrami operator (LBO) over a surface [33]. Let M be a triangular discretization of an arbitrary surface $\mathcal{S}$, $\{\mathbf{x}_i\}_{i=1}^N$ be the vertex set of M with N points, and $N_1(i) = \{i_1, i_2, \ldots, i_n\}$ be the set of vertex indices of one-ring neighbors of $\mathbf{x}_i$ with $i_1 = i_n$ (see Fig. 1(b)). For simplicity, let $\phi_i = \phi(\mathbf{x}_i)$ and T_j be a triangle with vertices $\mathbf{x}_i$, $\mathbf{x}_j$, and $\mathbf{x}_{j+}$, shown in Fig. 1(c).

The gradient on triangle T_j can be approximated by

$$\begin{aligned}\nabla_{T_j}\phi = \frac{1}{4A_j^2}\big\{&\phi_i[\gamma(\mathbf{x}_i,\mathbf{x}_j,\mathbf{x}_{j+}) + \gamma(\mathbf{x}_i,\mathbf{x}_{j+},\mathbf{x}_j)]\\ &+\phi_j[\gamma(\mathbf{x}_j,\mathbf{x}_i,\mathbf{x}_{j+}) + \gamma(\mathbf{x}_j,\mathbf{x}_{j+},\mathbf{x}_i)]\\ &+\phi_{j+}[\gamma(\mathbf{x}_{j+},\mathbf{x}_j,\mathbf{x}_i) + \gamma(\mathbf{x}_{j+},\mathbf{x}_i,\mathbf{x}_j)]\big\},\end{aligned} \tag{2.1}$$

where A_j is the area of T_j and

$$\gamma(\mathbf{x}_i,\mathbf{x}_j,\mathbf{x}_k) = \langle \mathbf{x}_i - \mathbf{x}_j, \mathbf{x}_j - \mathbf{x}_k\rangle\,(\mathbf{x}_k - \mathbf{x}_i).$$

Here, $< \mathbf{a}, \mathbf{b} >$ is the inner product of two vectors. The discrete gradient at vertex $\mathbf{x}_i$ is defined as a weighted average of the gradients on the neighboring triangles of $\mathbf{x}_i$

$$\nabla_M\phi_i = \frac{1}{\mathcal{A}(\mathbf{x}_i)}\sum_{j\in N_1(i)} A_j\nabla_{T_j}\phi, \tag{2.2}$$

where the area is given as $\mathcal{A}(\mathbf{x}_i) = \sum_{j\in N_1(i)} A_j$, shown in Fig. 1(b). Then, the numerical approximation at vertex $\mathbf{x}_i$ for the Laplacian over surface $\mathcal{S}$ can be defined as

$$\Delta_{\mathcal{S}}\phi_i \approx \Delta_M\phi_i = \frac{1}{2\mathcal{A}(\mathbf{x}_i)}\sum_{j\in N_1(i)} \mathbf{n}_j^T[\nabla_M\phi_j + \nabla_M\phi_{j+}]\,\|\mathbf{x}_j - \mathbf{x}_{j+}\|, \tag{2.3}$$

where $\mathbf{n}_j$ is the unit outward normal to edge $\overline{\mathbf{x}_j\mathbf{x}_{j+}}$. Since $\mathbf{n}_j$ is perpendicular to $\overline{\mathbf{x}_j\mathbf{x}_{j+}}$, $< \mathbf{n}_j, \overline{\mathbf{x}_j\mathbf{x}_{j+}} >= 0$. Here, two vectors, $\mathbf{n}_j$ and $\overline{\mathbf{x}_j\mathbf{x}_{j+}}$, can be expressed as combinations

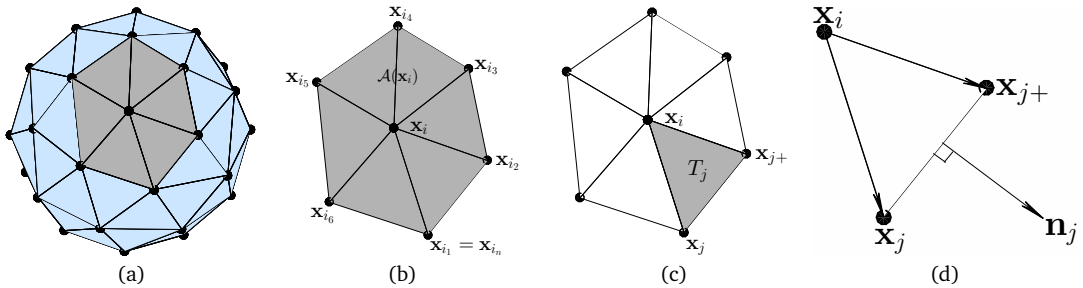

(a) (b) (c) (d)

Figure 1: Schematic of (a) triangular surface, (b) set of vertices of one-ring neighbors x_i and area $\mathcal{A}(x_i)$, (c) triangle T_j with verticesx_i, x_j, x_{j+}, and (d) unit normal vector $\mathbf{n}_j$.

of $\mathbf{u}$ and $\mathbf{v}$. Thus, $< s\mathbf{u} + (1-s)\mathbf{v},\ \mathbf{u} - \mathbf{v} >= 0$. It is given as

$$\mathbf{n}_j = \frac{s\mathbf{u} + (1-s)\mathbf{v}}{\|s\mathbf{u} + (1-s)\mathbf{v}\|},$$

where $s =< \mathbf{v},\ \mathbf{v} - \mathbf{u} > /\|\mathbf{u} - \mathbf{v}\|^2$, $\mathbf{u} = \mathbf{x}_j - \mathbf{x}_i$, and $\mathbf{v} = \mathbf{x}_{j+} - \mathbf{x}_i$, see Fig. 1(d).

Let $\phi_i^n = \phi(\mathbf{x}_i, n\Delta t)$, where Δt is the time step. Then, the proposed numerical method for the surface AC equation is as follows: First, we solve the diffusion term using the explicit Euler method

$$\frac{\phi_i^* - \phi_i^n}{\Delta t} = \Delta_M \phi_i^n, \quad 1 \le i \le N \tag{2.4}$$

and then solve the reaction term using the closed-form solution obtained from separation of variables

$$\phi_i^{n+1,*} = \frac{\phi_i^*}{\sqrt{[1-(\phi_i^*)^2]e^{-2\Delta t/\epsilon^2} + (\phi_i^*)^2}} \quad \text{for} \quad 1 \le i \le N. \tag{2.5}$$

Let $\phi_i^{n+1} = \phi_i^{n+1,*}$ be the numerical solution at time $t = (n+1)\Delta t$ for the surface AC equation. Refer to [6, 13] for more details about the explicit hybrid numerical scheme for the AC equation.

Next, for the numerical solution for the surface CAC equation, we take one more following step in addition to Eq. (2.5):

$$\phi_i^{n+1} = \phi_i^{n+1,*} + \beta\sqrt{F\big(\phi_i^{n+1,*}\big)}, \tag{2.6}$$

where β is defined so as to satisfy the total mass conservation constraint, i.e.,

$$\sum_{i=1}^{N} \phi_i^{n+1} \frac{\mathcal{A}(\mathbf{x}_i)}{3} = \sum_{i=1}^{N} \phi_i^0 \frac{\mathcal{A}(\mathbf{x}_i)}{3}. \tag{2.7}$$

Therefore, β is defined as

$$\beta = \frac{\sum\limits_{i=1}^{N} \big(\phi_i^0 - \phi_i^{n+1,*}\big)\mathcal{A}(\mathbf{x}_i)}{\sum\limits_{i=1}^{N} \sqrt{F\big(\phi_i^{n+1,*}\big)}\mathcal{A}(\mathbf{x}_i)}. \tag{2.8}$$

We also note that we use an operator splitting method with an explicit time-stepping scheme, although there are many monolithic and implicit methods for the AC-type equations that have been considered in the literature. As demonstrated in [13], an explicit scheme for the AC-type equations is better than an implicit scheme when we consider the accuracy of the numerical solutions under an equivalent computational cost.

3. Numerical experiments

In this section, we perform various numerical experiments to demonstrate the efficiency and accuracy of the proposed scheme. For the triangular mesh, we use DistMesh; it is a MATLAB algorithm of the mesh generator [26] which was used in various studies [3, 24]. Let h_{ave} be the average length of sides of triangles. First, we compare the numerical Laplacian with spherical and toroidal Laplacian.

3.1. Comparison between numerical and spherical Laplacians

We consider a unit sphere $\mathcal{S}$ consisting of points (x, y, z) in three-dimensional Cartesian coordinates $\mathbf{R}^3$: $x = \sin\psi\cos\theta$, $y = \sin\psi\sin\theta$, $z = \cos\psi$. Here, θ is the azimuthal angle with $0 \le \theta < 2\pi$ and ψ is the polar angle with $0 \le \psi \le \pi$. Using the DistMesh algorithm, we make the following discrete unit sphere with a triangular mesh, as shown in Fig. 2.

Let us consider a spherical Laplacian

$$\Delta_{\mathcal{S}}\phi = \frac{1}{\sin^2\psi}\frac{\partial^2\phi}{\partial\theta^2} + \frac{1}{\sin\psi}\frac{\partial}{\partial\psi}\left(\sin\psi\frac{\partial\phi}{\partial\psi}\right). \tag{3.1}$$

Then, we obtain the following spherical Laplacian for $\phi = z$ and z^2, respectively:

$$\Delta_{\mathcal{S}} z = -2z, \tag{3.2}$$

$$\Delta_{\mathcal{S}} z^2 = 2 - 6z^2. \tag{3.3}$$

Fig. 3 presents the results from the numerical Laplacian (2.3) and spherical Laplacian (3.2), (3.3) for (a) $\phi = z$ and (b) $\phi = z^2$. It is observed that the numerical results become close to the theoretical values with the reduction in mesh size h_{ave}.

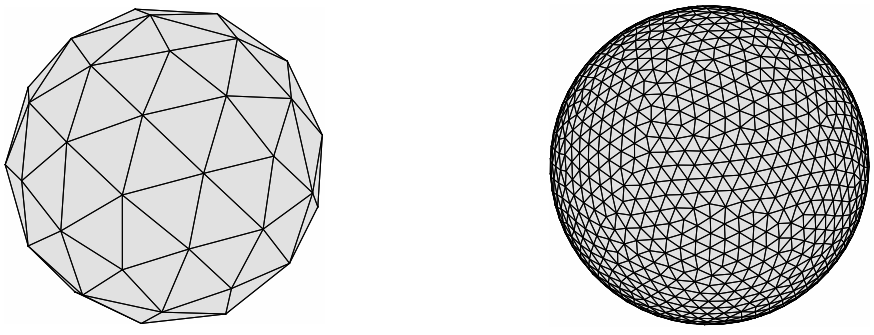

(a) (b)

Figure 2: Discrete unit sphere for (a) $h_{ave} = 0.5163$ and (b) $h_{ave} = 0.1055$.

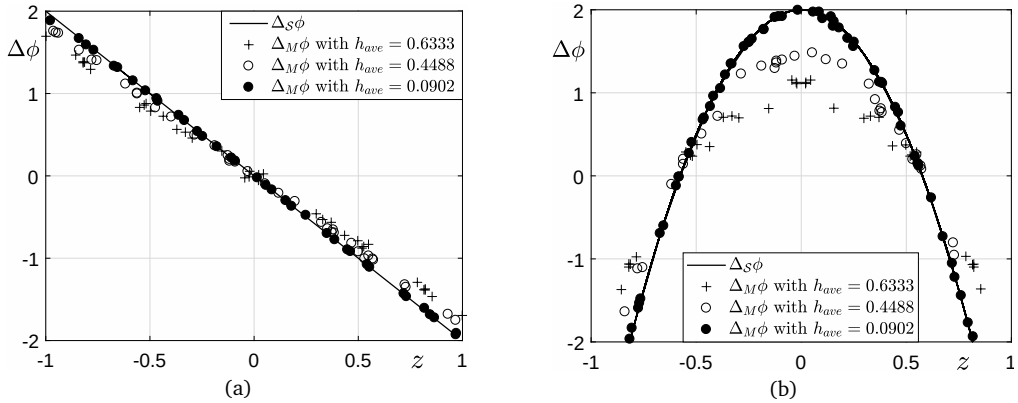

Figure 3: Comparison between the spherical Laplacian Δ_S and the numerical Laplacian Δ_M for each h_{ave}. Here, (a) $\phi = z$ and (b) $\phi = z^2$ are used.

We define the discrete L_2-norm as

$$\|\phi\|_2 = \left(\frac{\sum_{i=1}^{N} \phi_i^2 \mathcal{A}(\mathbf{x}_i)}{\sum_{i=1}^{N} \mathcal{A}(\mathbf{x}_i)} \right)^{\frac{1}{2}} \tag{3.4}$$

and a relative error as

$$E_{h_{ave}} = \frac{\|\Delta_S\phi - \Delta_M\phi\|_2}{\|\Delta_S\phi\|_2}. \tag{3.5}$$

The rate of convergence is defined as

$$\frac{\log\left(\frac{E_{h_{ave}}}{E_{h'_{ave}}}\right)}{\log\left(\frac{h_{ave}}{h'_{ave}}\right)}, \tag{3.6}$$

where h'_{ave} is a finer grid size than h_{ave}. Table 1 lists the L_2-norm error and the rate of convergence. The result shows that the L_2-norm errors decrease as h_{ave} reduces. Moreover, the convergence rates are between 1 and 2.

Table 1: L_2-norm errors and convergence rates with respect to h_{ave}.

Case (h_{ave})	0.4488	Rate	0.3890	Rate	0.2719	Rate	0.1935
$\phi = z$	0.0858	1.41	0.0702	1.82	0.0366	1.93	0.0190
$\phi = z^2$	0.2524	1.29	0.2099	1.84	0.1087	1.98	0.0555

3.2. Comparison between the numerical and toroidal Laplacians

Let $\mathcal{S}$ be a torus surface with R, the distance from the center of the tube to the center of the torus, and r, the radius of the tube, $0 < r < R$. We define the angle

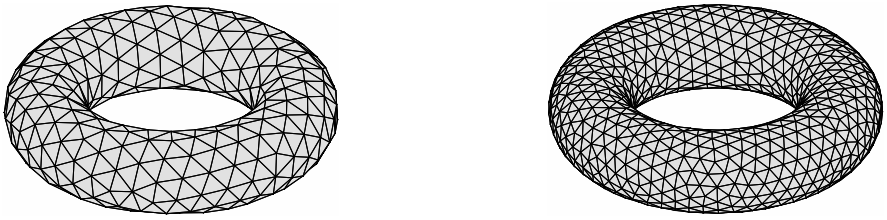

(a) (b)

Figure 4: Discrete torus for (a) $h_{ave} = 0.6164$ and (b) $h_{ave} = 0.3838$.

$0 \leq \theta, \psi \leq 2\pi$. The surface of torus $\mathcal{S}$ consists of points (x, y, z) in three-dimensional Cartesian coordinates $\mathbf{R}^3$, where

$$x = (R - r\cos\psi)\cos\theta, \quad y = (R - r\cos\psi)\sin\theta, \quad z = r\sin\psi.$$

We study the motion by mean curvature on a surface of ring torus $\mathcal{S}$. In Fig 4, we set the radii at $R = 3$ and $r = 1$.

Now, we consider the following toroidal Laplacian [10]:

$$\Delta_{\mathcal{S}}\phi = \frac{1}{(R - r\cos\psi)^2}\frac{\partial^2\phi}{\partial\theta^2} + \frac{1}{r^2(R - r\cos\psi)}\frac{\partial}{\partial\psi}\left((R - r\cos\psi)\frac{\partial\phi}{\partial\psi}\right). \tag{3.7}$$

Then, we obtain the following toroidal Laplacians for $\phi = z$, and z^2, respectively:

$$\Delta_{\mathcal{S}} z = \frac{z}{r^2\rho}(R - 2\rho), \tag{3.8}$$

$$\Delta_{\mathcal{S}} z^2 = \frac{2}{r^2\rho}\left(r^2\rho + (R - 3\rho)z^2\right), \tag{3.9}$$

where $\rho = \sqrt{x^2 + y^2}$. For $\phi = z$ and $\phi = z^2$, we compare the numerical Laplacian (2.3) and toroidal Laplacian (3.8), (3.9). Fig. 5 shows that the smaller the h_{ave} taken, the more accurate are the numerical results.

Table 2 represents the L_2-norm errors and convergence rates using Eqs. (3.5) and (3.6). The L_2-norm errors decrease as the h_{ave} becomes smaller, and the convergence rates are between 1 and 2.

Table 2: l_2 norm errors and the convergence rates with $\phi = z$ and z^2.

Case (h_{ave})	0.5547	Rate	0.4502	Rate	0.3658	Rate	0.2779
$\phi = z$	0.1342	1.87	0.0908	1.73	0.0635	1.76	0.0391
$\phi = z^2$	0.3154	1.74	0.2193	1.80	0.1508	1.81	0.0918

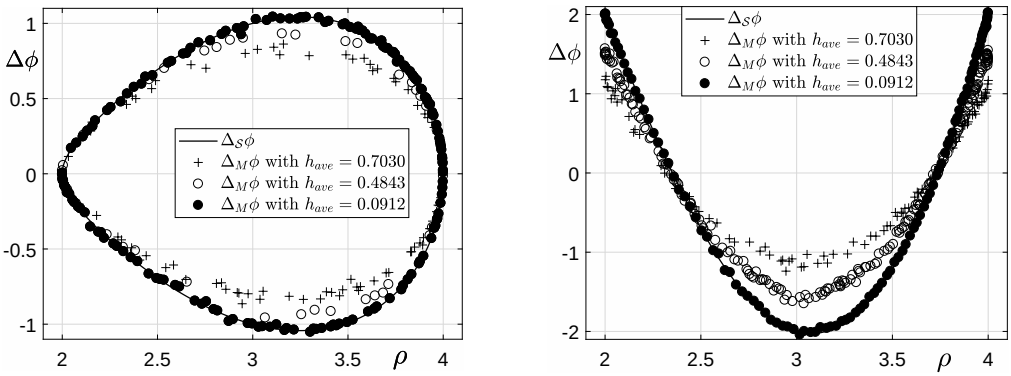

(a) (b)

Figure 5: Comparison between the toroidal Laplacian $\Delta_{\mathcal{S}}$ and the numerical Laplacian Δ_M for each h_{ave}: (a) $\phi = z$ and (b) $\phi = z^2$. Here, $R = 3$ and $r = 1$ are used.

3.3. Allen-Cahn equation

We consider the motion by mean curvature on a sphere. The analytic solution [6] is obtained using the concepts of curvature and tangential component

$$r(t) = \sqrt{R^2 - (R^2 - r_0^2)\, e^{2t/R^2}}, \tag{3.10}$$

where $R = 1$ is the radius of sphere, $r(t)$ is the radius of the spherical cap at time t, and r_0 is the initial radius of the spherical cap. In Fig. 6, the initial condition is defined as

$$\phi = \tanh \frac{\sqrt{x^2 + y^2} - z}{\sqrt{2}\epsilon} \tag{3.11}$$

and we set the initial radius $r_0 = 0.7064$, time step $\Delta t = 1.0e\text{-}5$, and $\epsilon = 0.3$. Fig. 6 presents the temporal evolution of surface view for time (a) $t = 0$, (b) $t = 10000\Delta t$, and (c) $t = 20000\Delta t$. The black solid line represents the circle that is set with the zero values. As time goes on, the circle radius indicated by the black line shrinks according to the motion by mean curvature.

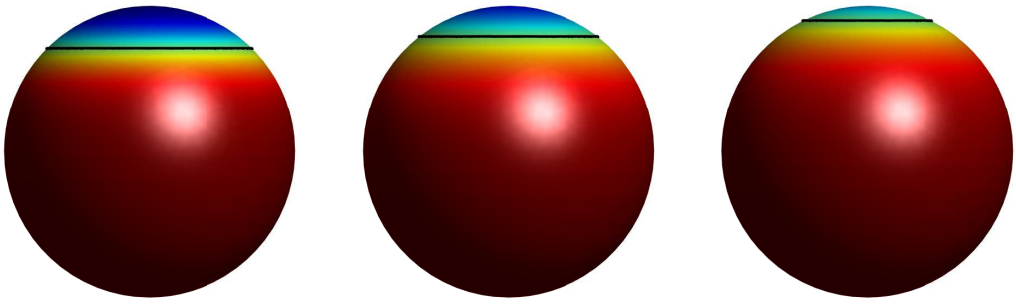

(a) (b) (c)

Figure 6: Temporal evolution: (a) initial condition, (b) $t = 10000\Delta t$, and (c) $t = 20000\Delta t$.

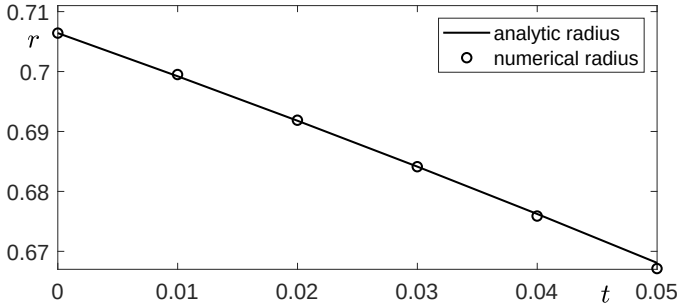

Figure 7: Comparison between analytic radius and numerical radius.

Fig. 7 shows the change in length of the radius over time. The solid line represents the calculation of Eq. (3.10), and the circle symbol indicates the numerical radius over the evolution of time. The decreasing numerical radius over time is approximately equal to the analytic radius.

The discrete total energy is defined as

$$\mathcal{E}_d(\phi) = \sum_{i=1}^{N} \left(\frac{F(\phi_i)}{\epsilon^2} + \frac{|\nabla_M \phi_i|^2}{2} \right) \frac{\mathcal{A}(\mathbf{x}_i)}{3}. \tag{3.12}$$

Fig. 8 illustrates the normalized discrete total energy over time with the initial condition (3.11) and the same parameters as those in the earlier test were used. We verify that the total energy decreases monotonically from the numerical result.

Next, we consider the convergence of the surface AC equation. Let

$$\phi(x, y, z, t) = z^2 \cos(t) \tag{3.13}$$

be a manufactured solution for the following surface AC equation with a source term:

$$\frac{\partial \phi(\mathbf{x}, t)}{\partial t} = -\frac{F'(\phi(\mathbf{x}, t))}{\epsilon^2} + \Delta_{\mathcal{S}} \phi(\mathbf{x}, t) + f(\mathbf{x}, t), \quad \mathbf{x} \in \mathcal{S}, \quad t > 0. \tag{3.14}$$

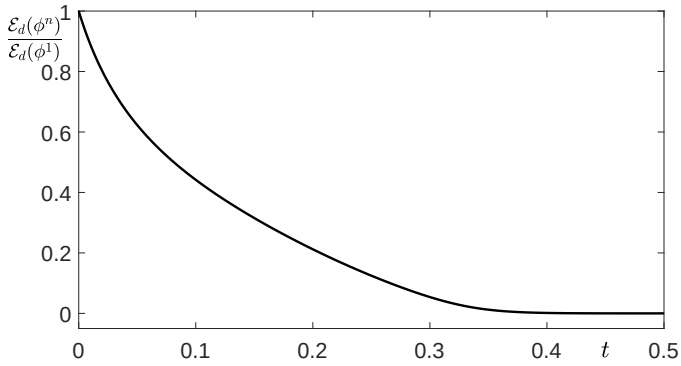

Figure 8: Decrease in discrete total energy over time.

Therefore, the source term is defined as

$$f(\mathbf{x},t) = \frac{\partial\phi(\mathbf{x},t)}{\partial t} + \frac{F'(\phi(\mathbf{x},t))}{\epsilon^2} - \Delta_{\mathcal{S}}\phi(\mathbf{x},t)$$
$$= -z^2\sin(t) + \frac{F'(z^2\cos(t))}{\epsilon^2} + \big(6z^2-2\big)\cos(t).$$

The initial condition is $\phi(x,y,z,0) = z^2$ and the parameters are $\Delta t = 1.0e$-5 and $\epsilon = 0.3$. After 100 iterations, the L_2-norm errors and convergence rates are listed in Table 3. We calculate the L_2-norm errors by decreasing h_{ave} and the convergence rates. Table 3 shows that the convergence rates are between 1 and 2.

Table 3: L_2-norm errors and the convergence rates with respect to h_{ave}.

Case (h_{ave})	0.4488	Rate	0.3895	Rate	0.2719	Rate	0.1783
$\phi = z^2$	$1.0482e$-3	1.44	$8.5801e$-4	1.89	$4.3319e$-4	1.87	$1.9690e$-4

3.4. Conservative Allen-Cahn equation

We solve the CAC equation in this test with the same simulation parameters that were used in Fig. 6. To set a smooth initial condition, we choose it as the result of Eq. (3.11) at $t = 2000\Delta t$. We use the time step $\Delta t = 1.0e$-6, thickness of transition layer $\epsilon = 0.1$, $h_{\text{ave}} = 0.044$, and initial radius $r = 0.7069$. Fig. 9 shows the temporal evolution for (a) initial condition and (c) $t = 2000\Delta t$. Fig. 9(b) represents the changes in radius and normalized mass for each iteration. We inferred that mass is conserved, and the radius is retained. In Fig. 10, we used the same parameters as the Fig. 9 except the initial condition. The initial condition is defined as

$$\phi(x,y,z,0) = \tanh\left(\frac{\max(|x|-0.5, |z-1|-0.5)}{\sqrt{2}\epsilon}\right). \tag{3.15}$$

Eq. (3.15) represents the modified rectangular shape on the unit spheres as shown in Fig. 10(a). Figs. 10(b), 10(c), and 10(d) show the shape of rounded rectangular, ellipsoidal, and circular on the unit sphere, respectively, with time evolution.

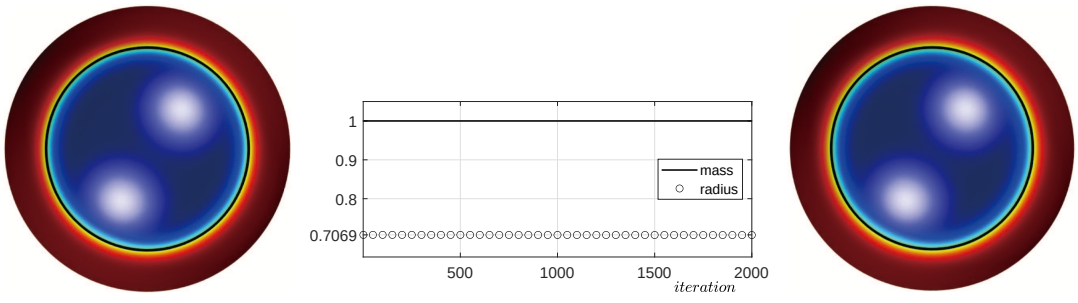

(a) (b) (c)

Figure 9: (a) Initial condition, (b) changes in mass and radius for each iteration, and (c) $t = 2000\Delta t$.

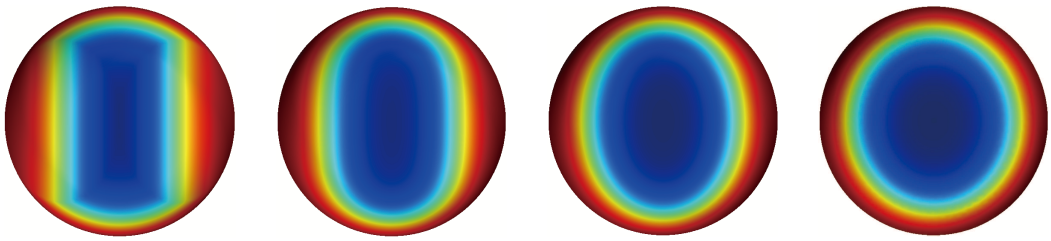

(a) (b) (c) (d)

Figure 10: Temporal evolutions with the rectangle shape $\phi(x, y, z, t)$ on the unit sphere: (a) initial condition, (b) $5000\Delta t$, (c) $15000\Delta t$, and (d) $35000\Delta t$.

4. Conclusions

In this study, we presented a simple and fast explicit hybrid numerical scheme for motion by mean curvature on a surface in 3D space. We numerically solve the AC and CAC equations on a triangular surface mesh. The proposed numerical method is computationally fast and efficient because we use an explicit hybrid numerical scheme. We performed various numerical experiments to demonstrate the robustness and efficiency of the proposed scheme. In future work, we will extend the proposed method to include fluid flows so that we can simulate the multi-phase fluid flows on curved surfaces.

Acknowledgments

The authors thank the reviewers for the constructive and helpful comments on the revision of this article.

Y. Choi was supported by the National Research Foundation of Korea (NRF) grant funded by the Korea government (NRF-2020R1C1C1A0101153712). Y. Li was supported by the Fundamental Research Funds for Central Universities (XTR 042019005) and the China Postdoctoral Science Foundation (2018M640968). C. Lee was supported by Basic Science Research Program through the National Research Foundation of Korea funded by the Ministry of Education (NRF-2019R1A6A3A13094308). H. Kim was supported by Basic Science Research Program through the National Research Foundation of Korea funded by the Ministry of Education (NRF-2020R1A6A3A13077105). J. Kim was supported by Basic Science Research Program through the National Research Foundation of Korea funded by the Ministry of Education (NRF-2019R1A2C1003053).

References

[1] S. M. Allen and J. W. Cahn, *A microscopic theory for antiphase boundary motion and its application to antiphase domain coarsening*, Acta Metallurgica, 27(6) (1979) 1085–1095.

[2] H. Biddle, I. von Glehn, C. B. Macdonald and T. Marz, *A volume-based method for denoising on curved surfaces*, Image Processing (ICIP), 2013 20th IEEE International Conference on. IEEE, 2013.
[3] B. Bogosel, *Efficient algorithm for optimizing spectral partitions*, Appl. Math. Comput., 333 (2018) 61–75.
[4] M. Brassel and E. Bretin, *A modified phase field approximation for mean curvature flow with conservation of the volume*, Math. Methods Appl. Sci., 10(34) (2011) 1157–1180.
[5] E. Celiker and P. Lin, *An efficient finite element method with exponential mesh refinement for the solution of the Allen–Cahn equation in non-convex polygons*, Commu. Comput. Phys., 28(4) (2020) 1536–1560.
[6] Y. Choi, D. Jeong, S. Lee, M. Yoo and J. Kim, *Motion by mean curvature of curves on surfaces using the Allen-Cahn equation*, Internat. J. Eng. Sci., 97 (2015) 126–132.
[7] P. Colli, T. Fukao and K. F. Lam, *On a coupled bulk-surface Allen-Cahn system with an affine linear transmission condition and its approximation by a Robin boundary condition*, Nonlinear Anal., 184 (2019) 116–147.
[8] G. Dziuk and C. M. Elliott, *Surface finite elements for parabolic equations*, J. Comput. Math., (2007) 385–407.
[9] H. Egger, K. Fellner, J.-F. Pietschmann and B. Q. Tang, *Analysis and numerical solution of coupled volume-surface reaction-diffusion systems with application to cell biology*, Appl. Math. Comput., 336 (2018) 351–367.
[10] C. C. Green and J. S. Marshall, *Green's function for the Laplace-Beltrami operator on a toroidal surface*, Proc. R. Soc. A, 2149 (2013) 469–479.
[11] P. Hansbo, M. G. Larson and A. Massing, *A stabilized cut finite element method for the Darcy problem on surfaces*, Comput. Methods Appl. Mech. Eng., 326 (2017) 298–318.
[12] Q. A. Huang, W. Jiang and J. Z. Yang, *An efficient and unconditionally energy stable scheme for simulating solid-state dewetting of thin films with isotropic surface energy*, Commu. Comput. Phys., 26 (2019) 1444–1470.
[13] D. Jeong and J. Kim, *An explicit hybrid finite difference scheme for the Allen-Cahn equation*, J. Comput. Appl. Math., 340 (2018) 247–255.
[14] D. Jeong, Y. Li, Y. Choi, M. Yoo, D. Kang, J. Park, J. Choi and J. Kim, *Numerical simulation of the zebra pattern formation on a three-dimensional model*, Phys. A, 475 (2017) 106–116.
[15] D. Jeong, Y. Li, C. Lee, J. Yang and J. Kim, *A conservative numerical method for the Cahn-Hilliard equation with generalized mobilities on curved surfaces in three-dimensional space*, Commu. Comput. Phys., 27(2) (2020) 412–430.
[16] J. Kim, D. Jeong, S.-D. Yang and Y. Choi, *A finite difference method for a conservative Allen-Cahn equation on non-flat surfaces*, J. Comput. Phys., 334 (2017) 170–181.
[17] K. F. Lam and H. Wu, *Convergence to equilibrium for a bulk-surface Allen-Cahn system coupled through a nonlinear Robin boundary condition*, Discrete Contin. Dyn. Syst. Ser. A, 40(3) (2020) 1847.
[18] Y. Li, X. Qi and J. Kim, *Direct discretization method for the Cahn-Hilliard equation on an evolving surface*, J. Sci. Comput., 77(2) (2018) 1147–1163.
[19] C. B. Macdonald and S. J. Ruuth, *The implicit closest point method for the numerical solution of partial differential equations on surfaces*, SIAM J. Sci. Comput., 31(6) (2009) 4330–4350.
[20] D. Marenduzzo and E. Orlandini, *Phase separation dynamics on curved surfaces*, Soft Matter, 9(4) (2013) 1178–1187.
[21] T. Marz and C. B. Macdonald, *Calculus on surfaces with general closest point functions*,

SIAM J. Numer. Anal., 50(6) (2012) 3303–3328.
[22] B. MERRIMAN AND S. J. RUUTH, *Diffusion generated motion of curves on surfaces*, J. Comput. Phys., 225(2) (2007) 2267–2282.
[23] V. MOHAMMADI, D. MIRZAEI AND M. DEHGHAN, *Numerical simulation and error estimation of the time-dependent Allen-Cahn equation on surfaces with radial basis functions*, J. Sci. Comput., 79(1) (2019) 493–516.
[24] D. T. OANH, O. DAVYDOV AND H. X. PHU, *Adaptive RBF-FD method for elliptic problems with point singularities in 2D*, Appl. Math. Comput., 313 (2017) 474–497.
[25] A. S. PATELLI, L. DEDÉ, T. LASSILA, A. BARTEZZAGHI AND A. QUARTERONI, *Isogeometric approximation of cardiac electrophysiology models on surfaces: An accuracy study with application to the human left atrium*, Comput. Methods Appl. Mech. Eng., 317 (2017) 248–273.
[26] P. O. PERSSON, *DistMesh*, `http://persson.berkeley.edu/distmesh/`
[27] G. PITTON AND L. HELTAI, *NURBS-SEM: A hybrid spectral element method on NURBS maps for the solution of elliptic PDEs on surfaces*, Comput. Methods Appl. Mech. Eng., 338 (2018) 440–462.
[28] P. TANG, F. QIU, H. ZHANG AND Y. YANG, *Phase separation patterns for diblock copolymers on spherical surfaces: A finite volume method*, Phys. Rev. E, 72(1) (2005) 016710.
[29] G. TURK, *Generating textures on arbitrary surfaces using reaction-diffusion*, ACM SIGGRAPH Computer Graphics, 25(4) (1991) 289–298.
[30] B. XIA, Y. LI AND Z. LI, *Second-order unconditionally stable direct methods for Allen-Cahn and conservative Allen-Cahn equations on surfaces*, Mathematics, 8(9) (2020) 1486.
[31] X. XIAO, X. FENG AND J. YUAN, *The stabilized semi-implicit finite element method for the surface Allen-Cahn equation*, Discrete Contin. Dyn. Syst. Ser B, 22(7) (2017) 2857.
[32] X. XIAO, R. HE AND X. FENG, *Unconditionally maximum principle preserving finite element schemes for the surface Allen-Cahn type equations*, Numer. Methods Partial Differ. Equ., 36(2) (2020) 418–438.
[33] G. XU, *Discrete Laplace-Beltrami operators and their convergence*, Comput. Aided Geom. Des., 21(8) (2004) 767–784.
[34] C. ZIMMERMANN, D. TOSHNIWAL, C. M. LANDIS, T. J. HUGHES, K. K. MANDADAPU AND R. A. SAUER, *An isogeometric finite element formulation for phase transitions on deforming surfaces*, Comput. Methods Appl. Mech. Eng., 351 (2019) 441–477.